Dust radiative forcing in snow of the Upper Colorado River Basin: 2. Interannual variability in radiative forcing and snowmelt rates

S. McKenzie Skiles,[1,2] Thomas H. Painter,[1,2,3] Jeffrey S. Deems,[4,5] Ann C. Bryant,[6] and Christopher C. Landry[7]

Received 27 February 2012; revised 25 May 2012; accepted 7 June 2012; published 26 July 2012.

[1] Here we present the radiative and snowmelt impacts of dust deposition to snow cover using a 6-year energy balance record (2005–2010) at alpine and subalpine micrometeorological towers in the Senator Beck Basin Study Area (SBBSA) in southwestern Colorado, USA. These results follow from the measurements described in part I. We simulate the evolution of snow water equivalent at each station under scenarios of observed and dust-free conditions, and +2°C and +4°C melt-season temperature perturbations to these scenarios. Over the 6 years of record, daily mean dust radiative forcing ranged from 0 to 214 W m^{-2}, with hourly peaks up to 409 W m^{-2}. Mean springtime dust radiative forcings across the period ranged from 31 to 49 W m^{-2} at the alpine site and 45 to 75 W m^{-2} at the subalpine site, in turn shortening snow cover duration by 21 to 51 days. The dust-advanced loss of snow cover (days) is linearly related to total dust concentration at the end of snow cover, despite temporal variability in dust exposure and solar irradiance. Under clean snow conditions, the temperature increases shorten snow cover by 5–18 days, whereas in the presence of dust they only shorten snow duration by 0–6 days. Dust radiative forcing also causes faster and earlier peak snowmelt outflow with daily mean snowpack outflow doubling under the heaviest dust conditions. On average, snow cover at the towers is lost 2.5 days after peak outflow in dusty conditions, and 1–2 weeks after peak outflow in clean conditions.

Citation: Skiles, S. M., T. H. Painter, J. S. Deems, A. C. Bryant, and C. C. Landry (2012), Dust radiative forcing in snow of the Upper Colorado River Basin: 2. Interannual variability in radiative forcing and snowmelt rates, *Water Resour. Res.*, *48*, W07522, doi:10.1029/2012WR011986.

1. Introduction

[2] In part I of this paper [*Painter et al.*, 2012] we present the detailed energy balance measurements required for investigation of radiative impacts of desert dust in alpine and subalpine snow cover, using data collected at the Senator Beck Basin Study Area (SBBSA) in the San Juan Mountains of southwest Colorado. Previously, *Painter et al.* [2007] isolated the effects of dust from other controls and showed with a two-year data set that the acceleration of melt by the shortwave radiative forcing of dust results in a shortening of snow cover duration in southwest Colorado by 18–35 days. In the present study we expand on *Painter et al.* [2007] to encompass the full observation period at our study sites, from 2005 through 2010. Additionally, given that by 2050 temperature increases of 2°C–4°C are projected in this region [*Barnett and Pierce*, 2009], we model the sensitivity of snowmelt to increases in melt season temperature by which to understand the relative magnitudes of forcings by dust and atmospheric warming, separately and in combination.

[1]Department of Geography, University of California, Los Angeles, California, USA.
[2]Joint Institute for Regional Earth System Science and Engineering, University of California, Los Angeles, California, USA.
[3]Jet Propulsion Laboratory, California Institute of Technology, Pasadena, California, USA.
[4]National Snow and Ice Data Center, Boulder, Colorado, USA.
[5]NOAA Western Water Assessment, Boulder, Colorado, USA.
[6]Department of Geography, University of Utah, Salt Lake City, Utah, USA.
[7]Center for Snow and Avalanche Studies, Silverton, Colorado, USA.

Corresponding author: T. H. Painter, Jet Propulsion Laboratory, California Institute of Technology, 4800 Oak Grove Dr., Pasadena, CA 91109, USA. (thomas.painter@jpl.nasa.gov)

0043-1397/12/2012WR011986

2. Methods

2.1. Radiative Forcing

[3] Radiative forcing by dust in snow directly affects the snowpack through enhanced absorption of solar radiation by dust (direct effect), and indirectly through enhanced absorption by larger grain size due to acceleration of grain growth from the direct effect (first indirect effect) and by the earlier exposure of a darker substrate (second indirect effect) [*Hansen and Nazarenko*, 2004]. From the micrometeorological measurements discussed in part I of this paper, the range of dust radiative forcings is determined using the treatment described by *Painter et al.* [2007].

[4] We calculate minimum and maximum radiative forcing to account for the range of potential radiative forcing

due to dust. Minimum surface radiative forcing addresses the direct effect of dust in snow by accounting for the reduction of snow albedo in the visible wavelengths. The maximum radiative forcing includes both the direct effect and the first indirect effect ($i1$) by accounting for reduction in visible albedo due to dust and reductions in the near infrared/shortwave infrared (NIR/SWIR) albedo from increases in grain size. The maximum forcing also includes direct forcing from perturbation of snow albedo in the NIR [*Singh et al.*, 2010; *Painter*, 2011].

[5] Minimum surface radiative forcing $f_{d\min}$ (W m^{-2}) is calculated as

$$F_{d\min} = E_{\text{vis}}\Delta_{\text{vis}}, \tag{1}$$

where E_{vis} is the visible irradiance (W m^{-2}) determined from the difference between the broadband and NIR/SWIR irradiances, $\Delta_{\text{vis}} = 0.92 - a_{\text{vis}}$, a_{vis} is calculated visible albedo, and 0.92 is the observed mean visible albedo for relatively dust-free snow at our study sites (no midlatitude snow is completely free of aerosols) [*Painter et al.*, 2007].

[6] Maximum surface radiative forcing $F_{d\max+/1}$ is calculated as

$$F_{d\max+/1} = 0.5[E_{\text{vis}}\Delta_{\text{vis}} + E_{\text{NIR}/\text{NIR}}(1/\xi) - 1], \tag{2}$$

where

$$\xi = 1 - 1.689\Delta_{\text{vis}}\Delta_{\text{vis}} \leq 0.17,$$

$$\xi = 0.67\Delta_{\text{vis}} > 0.17,$$

E_{NIR} is the NIR/SWIR net shortwave flux, and a_{NIR} is the NIR/SWIR albedo. The latter empirical relationship was developed in SBBSA and gives the proportion of the change in NIR/SWIR albedo due to the presence of dust versus grain coarsening in the absence of dust [*Marks et al.*, 1998; *Painter et al.*, 2007].

2.2. Temperature Change

[7] The relative capacities of radiative forcing by dust and temperature increases to accelerate snowmelt are addressed by simulating snowmelt with uniform, hourly temperature perturbations of +2°C and +4°C during the melt season, with and without dust. An increase in temperature increases sensible heating and longwave irradiance to the snow surface. The change in sensible heating is directly related to the temperature increase, whereas the increase in longwave irradiance depends also on the fraction of sky that is cloud covered and the relative humidity (which in turn affect the atmospheric emissivity). Cloud cover fraction is a difficult variable to estimate, so we bracket increases in longwave irradiance with treatments of clear sky and complete cloud conditions.

[8] Perturbations to the clear sky longwave irradiance are calculated with the parameterization described by *Konzelmann et al.* [1994]:

$$L = [0.23 + 0.443(e_a/T_a)^{1/8}](\sigma T_a^4), \tag{3}$$

where e_a is vapor pressure (Pa), T_a is air temperature (K), and σ is the Stefan-Boltzmann constant (5.67×10^{-8} W m^{-2} K^{-4}). This represents the Stefan-Boltzmann equation where $0.23 + 0.443(e_a/T_a)^{1/8}$ is the clear sky emissivity, with 0.23 being emissivity under a completely dry atmosphere.

[9] Longwave irradiance from a completely cloud covered sky is primarily determined by the temperature of the cloud base. We determine the perturbation of longwave under cloud cover with the following relation [*Konzelmann et al.*, 1994]:

$$L = \{[0.23 + 0.443(e_a/T_a)^{1/8}](1 - n^3) + 0.963n^3\}\sigma T_a^4, \tag{4}$$

where n is the fractional cloud cover and all others are as above. When the cloud cover is treated as complete, $n = 1$, the relation collapses to

$$L = (0.963)\sigma T_a^4, \tag{5}$$

where 0.963 is the emissivity under complete cloud cover. The ideal longwave parameterization would utilize data at our sites, a relationship we are currently working on developing. Until then we use these physically based relations which were developed in Greenland but have also been shown to perform well in a glacier environment in northern Sweden [*Sedlar and Hock*, 2009].

2.3. Snowmelt Model

[10] We use the point snow energy balance model (SNOBAL) to calculate snowmelt and predict point runoff using SBBSA tower and snow plot data on snow properties, measurement heights and depths, and energy exchanges [*Marks and Dozier*, 1992; *Marks et al.*, 1992]. In the model, the snowpack is represented as two layers: a 25 cm surface layer where energy exchanges take place, and the remainder of the pack as an energy and mass storage layer. The model utilizes site elevation, measurement heights, roughness length, and initial snow state variables (snow depth, snow density, snow surface temperature, average snowpack temperature, and liquid water content) as starting inputs. Snow variables and measurement heights are then updated at each time step (Figure 1). Energy exchanges are calculated in the active upper layer and then energy transfer is determined for the snowpack as a whole, from which the energy available for phase changes in both layers is determined. Melt is computed once the cold content (energy required to bring the temperature of the snow to 0°C) reaches 0 J m^{-2}. The cold content (Q) is calculated using the following equation:

$$Q = \rho h c_s(T_0 - T^n), \tag{6}$$

where ρ is the snow density, h is the snow height, c_s is the specific heat of ice, T_0 is melting temperature (0°C or 273.15 K), and T^n is the snow temperature (in either °C or K, depending on units for melting temperature) [*Marks et al.*, 1998]. When the liquid water content in the snowpack exceeds the amount allowed by the maximum liquid water holding capacity, the ratio of the volume of water with the difference between the volume of snow and volume of ice, then evaporation and snowpack outflow are estimated from the lower layer [*Marks et al.*, 1998].

[11] For this study we ran the model over the springtime melt season. The starting snowpack conditions, or state

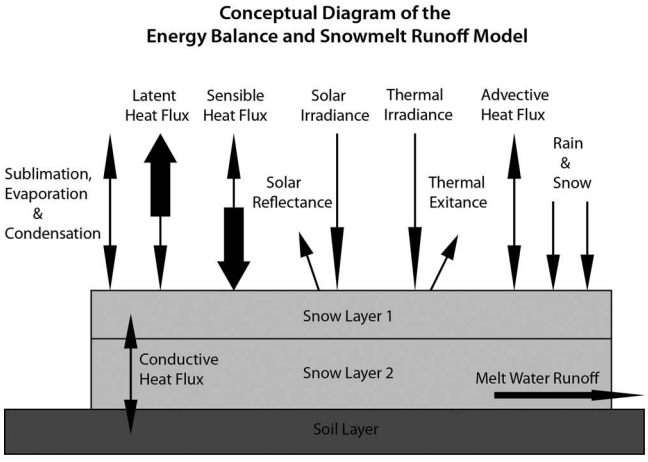

Figure 1. Conceptual diagram of SNOBAL model structure and components (after *Marks et al.* [1998]).

Table 2. SNOBAL Is Run for All Scenarios Shown in the First Column; the Scenario Results Shown in the Second Column are Scenario Means in Every Case But the Observed (D_0) Scenario

SNOBAL Scenarios	Results Scenarios
Dust (Observed)	D_0
Clean, maximum RF	
Clean, minimum RF	C_0
Dust +2°C, clear skies	
Dust +2°C, cloudy skies	D_2
Dust +4°C, clear skies	
Dust +4°C, cloudy skies	D_4
Clean Max +2°C, clear skies	
Clean Max +2°C, cloudy skies	
Clean Min +2°C, clear skies	
Clean Min +2°C, cloudy skies	C_2
Clean Max +4°C, clear skies	
Clean Max +4°C, cloudy skies	
Clean Min +4°C, clear skies	
Clean Min +4°C, cloudy skies	C_4

variables mentioned above, were determined from the manual snow measurements performed closest in time to 15 April (the date of average peak snow for the region) at each site. Changes in state variables, updated at an hourly time step, are driven by the observed forcing variables (hourly averages of net shortwave, longwave irradiance, air temperature, relative humidity, and wind speed), which are measured at the micrometeorological towers as described in part I of this paper (state and forcing variables summarized in Table 1). Soil temperature is set to 0°C for the model runs because the snow soil temperature is generally at or near 0°C in our observations and its flux to the snowpack is considered to have a negligible energy contribution [*Marks and Dozier*, 1992]. The model is used to predict snowmelt for 15 combinations of dust and temperature scenarios (Table 2). To simplify the presentation of our results we reduce the 15 sets of outputs to a set of six scenarios: observed conditions (D_0), observed conditions with dust radiative forcings removed (C_0), and each of these scenarios with the 2°C (D_2, C_2) and 4°C (D_4, C_4) temperature increases.

2.4. Sensitivity and Uncertainty

[12] SNOBAL has been shown to reproduce measured snowpack properties well [*Marks et al.*, 1998; *Painter et al.*, 2007], however measurement uncertainty and assumptions made in calculating energy flux in the model are unavoidable. We address the uncertainties for the tower instruments and the model sensitivity to parameter uncertainties by perturbing the values of each of the input parameters to the ranges in instrument uncertainty at the subalpine tower over the 2007 ablation season.

Table 1. SNOBAL Forcing Variables and Modeled State Variables (After *Marks* et al. [1998])

State Variables	Forcing Variables
Snow depth (m)	Net solar radiation (W m^{-2})
Snow density (kg m^{-3})	Incoming longwave radiation (W m^{-2})
Snow surface layer temperature (°C)	Air temperature (°C)
Average surface layer temperature (°C)	Vapor pressure (Pa)
Average snow liquid water content (%)	Wind speed (m s^{-1})

[13] Movement of air near the snow surface is influenced by surface roughness, which in turn influences turbulent exchange energy transfer. Snow surface roughness is not constant and varies at different scales, both spatial and temporal [*Brock et al.*, 2006; *Fassnacht et al.*, 2009]. Published roughness lengths for snow include 0.2 mm for fresh snow [*Poggi*, 1976], average of 1.9 mm for annual snow cover [*Pluss and Mazzoni*, 1994], and 1–12 mm for rough snow [*Jackson and Carroll*, 1978]. While dust in snow can have varying impacts on surface roughness, *Fassnacht et al.* [2009] found that deposited dust melts snow more uniformly, which decreases roughness relative to surrounding cleaner snow surfaces. *Rhodes et al.* [1987] also found this would be the case in areas where solar radiation dominates energy balance following Ball's normal trajectory theory [*Ball*, 1954].

[14] For this analysis surface roughness was altered from the default 1 mm value to 5 mm, 1 cm, and 5 cm to test the sensitivity of the model to this parameter. The high value of 5 cm is used only to assess the model sensitivity; a surface roughness of 5 cm at the study plots is highly unlikely given typically observed surface roughness for alpine snow cover and at our study plots, though this could be achieved in areas of large suncup development.

3. Results

3.1. Radiative Forcing

[15] We calculated maximum and minimum radiative forcing (RF) due to dust in snow from 15 March to the date of modeled clean snow-all-gone date (SAG), as described above. While snowpack cold content is consistently nonzero during the period 15 March to 15 April, dust radiative forcing tends to begin during this period. The average of the two RF scenarios is plotted as daily means along with dust events, observed precipitation, and snow depth (Figure 2). RF is typically lower at the alpine site where dust concentrations tend to be lower and albedo higher. Remote sensing analyses suggest that the alpine tower is situated in an area of lower dust concentrations relative to most of the surrounding alpine

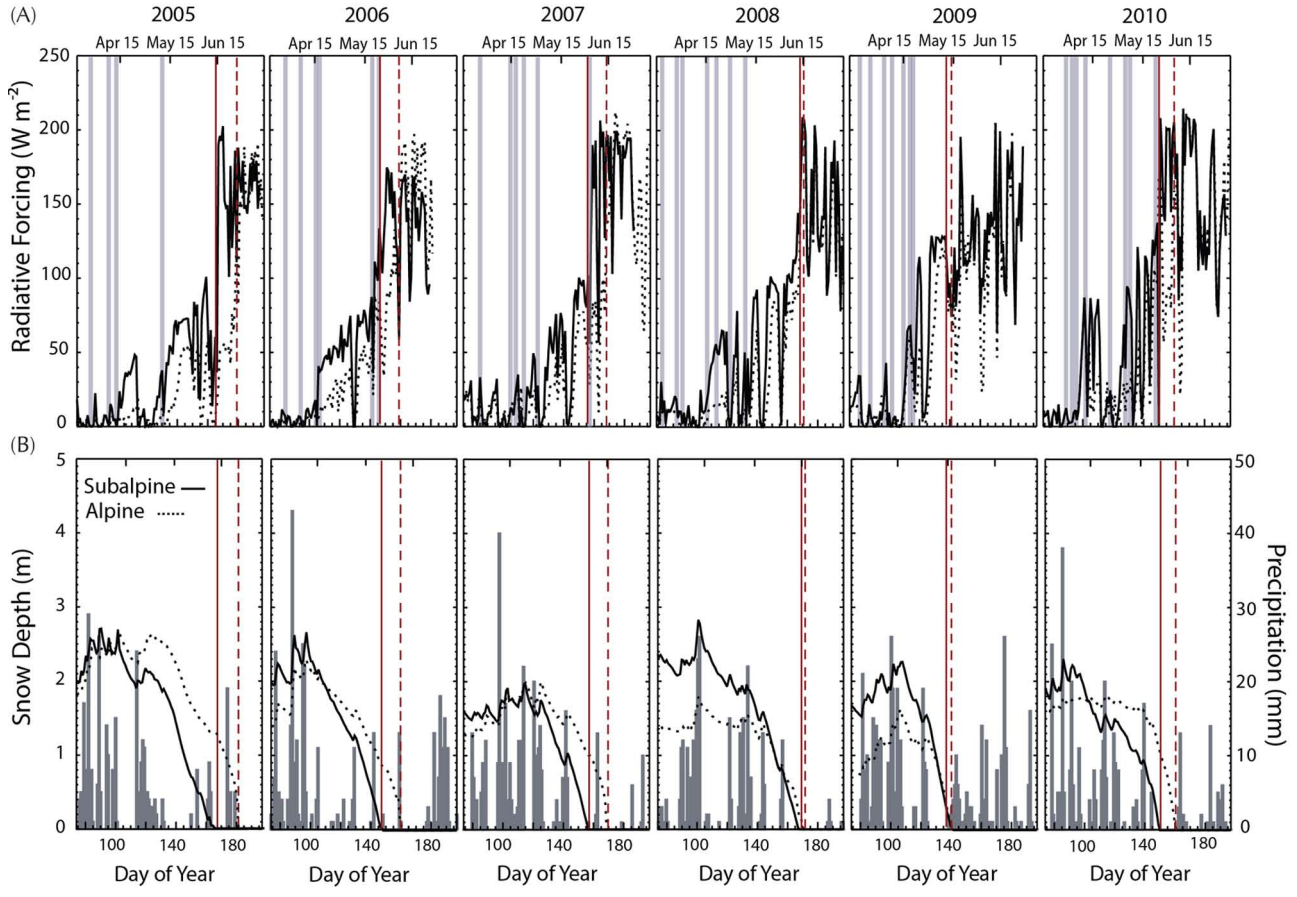

Figure 2. Time series of daily mean (a) dust radiative forcing, precipitation, and (b) snow depth at the subalpine (solid) and alpine (dashed) site from 15 March. Gray bars indicate a dust event and red bars indicate observed date of snow all gone (SAG) at each site.

terrain. This is most likely due to wind redistribution at this particularly windy site.

[16] RF varies on multiple temporal scales but typically increases after a dust event and decreases with a new snow precipitation event. Some dust events are accompanied by snowfall. In these cases the cleaner overlying new snow delays or reduces radiative forcing until the snow melts to a sufficiently low optical thickness that irradiance can interact with the dust layer. As the season advances, RF increases steadily as snow melts and previously buried dust layers converge at the snow surface.

[17] The year with the highest end of year dust concentration, 2009, also had the highest average mean daily RF over the ablation season, from 15 April to observed SAG, at 75 W m^{-2} at the subalpine site. This is a further 15 W m^{-2} over the next highest dust concentration year, 2010, and an additional 30 W m^{-2} over the lowest dust concentration year, 2005, which still had average RF of 45 W m^{-2}. The corresponding numbers at the alpine site are 50 W m^{-2} in 2009, an additional 7 W m^{-2} over 2010, and 33 W m^{-2} over 2005.

[18] Mean daily RF over the period from observed SAG (D_0) to modeled clean SAG (C_0) provides a measure of the contribution of the second indirect effect because the time between D_0 SAG and modeled C_0 SAG is when there would still be snow cover in the absence of dust. The RF varies over this period from 136 W m^{-2} (2006) to 150 W m^{-2} (2005), with an average of 144 W m^{-2}. Mean daily RF from 15 April to C_0 SAG, then, provides a measure of all effects, direct and both indirect effects. The daily mean RF over this period is again highest in 2009 with 114 W m^{-2} at the subalpine site and 84 W m^{-2} at the alpine site, for 2010, equivalent numbers of 100 and 81 W m^{-2}, and for 2005, 79 and 56 W m^{-2}. In all cases there is an additional 30–40 W m^{-2} of radiative forcing for the period of 15 April to C_0 SAG relative to D_0 SAG, this contribution coming from the time period when the snow is no longer on the ground, but would be in the absence of dust. The influence of this enhanced absorption on snow cover duration and melt is discussed below.

[19] In addition to variation in dust loading, variation in cloud cover, which impacts amount of incoming solar radiation, and new precipitation, which impacts the amount of time dust is exposed at the surface, over each spring season modulates calculated RF values (Figure 3). Springtime cumulative broadband irradiance, the total incoming solar radiation over the spring season between 15 April and 1 June, indicates interannual variability due to cloud cover. Over the whole record, changes in solar irradiance do not explain the difference in RF between high and low dust concentration years. For example, 2009 was a relatively cloudy spring with the lowest cumulative irradiance yet has the highest average springtime RF (Figure 3b).

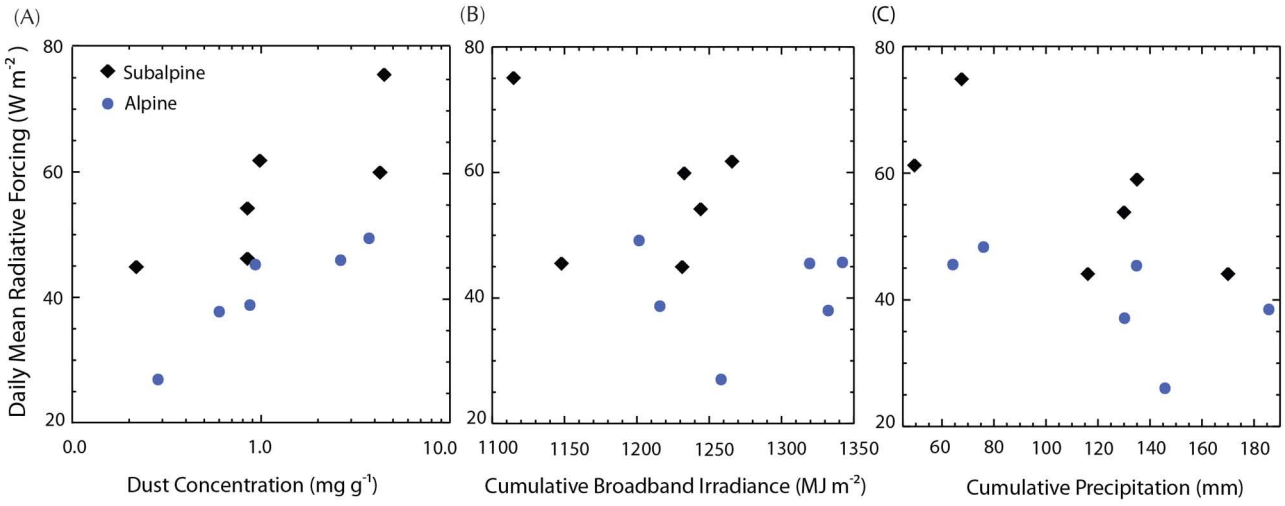

Figure 3. Daily mean radiative forcing with (a) end of year dust concentrations, (b) cumulative springtime broadband irradiance, and (c) cumulative springtime precipitation.

[20] New snowfall during the springtime season (15 April to D_0 SAG) dampens RF by increasing the snow albedo and temporarily isolating/reducing the interaction of irradiance with the dust layer. Daily mean RF shows a weakly negative relationship with cumulative springtime precipitation (Figure 3c). The combination of the three plots indicates that variable spring conditions do impact interannual variability in RF, with the majority of the variation due to total dust loading but modulated by springtime precipitation.

3.2. Longwave Irradiance and Turbulent Exchange

[21] Subalpine observed and modeled longwave irradiances are plotted (Figure 4) for increased temperature scenarios along with modeled sensible and latent heat fluxes for the D_0, D_2, and D_4 scenarios. The data from the alpine site (not shown) are very similar. Comparing Figure 4 with Figure 2 gives an indication of the magnitude of changes in fluxes due to temperature increase versus dust radiative forcing. Consistently across all years (2005–2010) and at both sites temperature increases of 2°C and 4°C increase daily mean longwave irradiance by averages of 8 and 16 W m^{-2}, respectively, and increase daily mean sensible heating by about 2 and 4 W m^{-2}, respectively. The impact on latent heat transfer is negligible, varying between ±1 W m^{-2} over all years. In comparison, in high dust concentration years enhanced surface shortwave absorption due to dust can be as high as 75 W m^{-2} (2009, subalpine site), and even in the lowest dust concentration year, 2005, dust enhanced shortwave absorption by 27 to 45 W m^{-2} (alpine, subalpine).

3.3. Model Accuracy

[22] We assess the SNOBAL accuracy according to its simulation of SAG and the time series of snow water equivalent relative to observations. For years 2005 through 2010, modeled SAG occurred within 1 day of observed SAG at both sites with the exception of the alpine site in 2005, when it was 2 days. This greater error resulted from inaccurate partitioning of precipitation phase during a rain on snow event at the end of the snow cover season.

[23] Measured SWE is closest to modeled SWE at the subalpine site, with a RMSE of 68 mm over all years (Figure 7). The difference between measured and modeled SWE was higher at the alpine site, with an RMSE of 119 mm over all years. The greater differences at the alpine site occur because snow depth has been observed to be consistently deeper in the snow pit plot than at the tower several meters away [*Painter et al.*, 2012]. The snow pit depths are greater by a mean of 20 cm (median 21 cm) and standard deviation of 7 cm over all years. If SWE is calculated using depth at the tower and mean pit density the result over all years is a mean difference of 90 mm. We use tower depth to calculate the plotted alpine SWE_m numbers (Figure 7) because we consider this to be more representative of the snowpack at the tower where the energy balance and radiation measurements are made. The magnitude of the variation could potentially induce uncertainties in the model results because the model is initiated with measurements from the snow pits, but forced with data measured at the tower.

3.4. Sensitivity and Uncertainty

[24] We modeled melt season SWE evolution for all individual parameters and their respective ranges in accuracy (Figure 5a). Individually, the greatest sensitivity of 2 days difference in SAG (ΔSAG) by the end of season occurred with the longwave irradiance, which has an instrument uncertainty of ±3%. The next largest change occurred for net solar radiation and wind with almost a l-day difference for each parameter. The sensitivities for air temperature, vapor pressure, and precipitation were negligible. SWE for all parameters accuracy ranges (Figure 5b) represents the maximum uncertainty involved with instrument measurements, which is 2 days ΔSAG for the maximum uncertainty range (+) and 3 days difference in SAG for the minimum uncertainty range (−).

[25] We plot the average ΔSAG with simulated changes in surface roughness at the subalpine and alpine sites (Figure 6). Due to model turbulent flux parameters snowmelt could not be simulated with a 5 cm surface roughness given the low wind speeds recorded at the subalpine site. For surface roughness of 5 mm in the dust case at both sites melt is either not impacted (subalpine), or advanced by 1 day (alpine). The largest difference in melt-out occurs for the

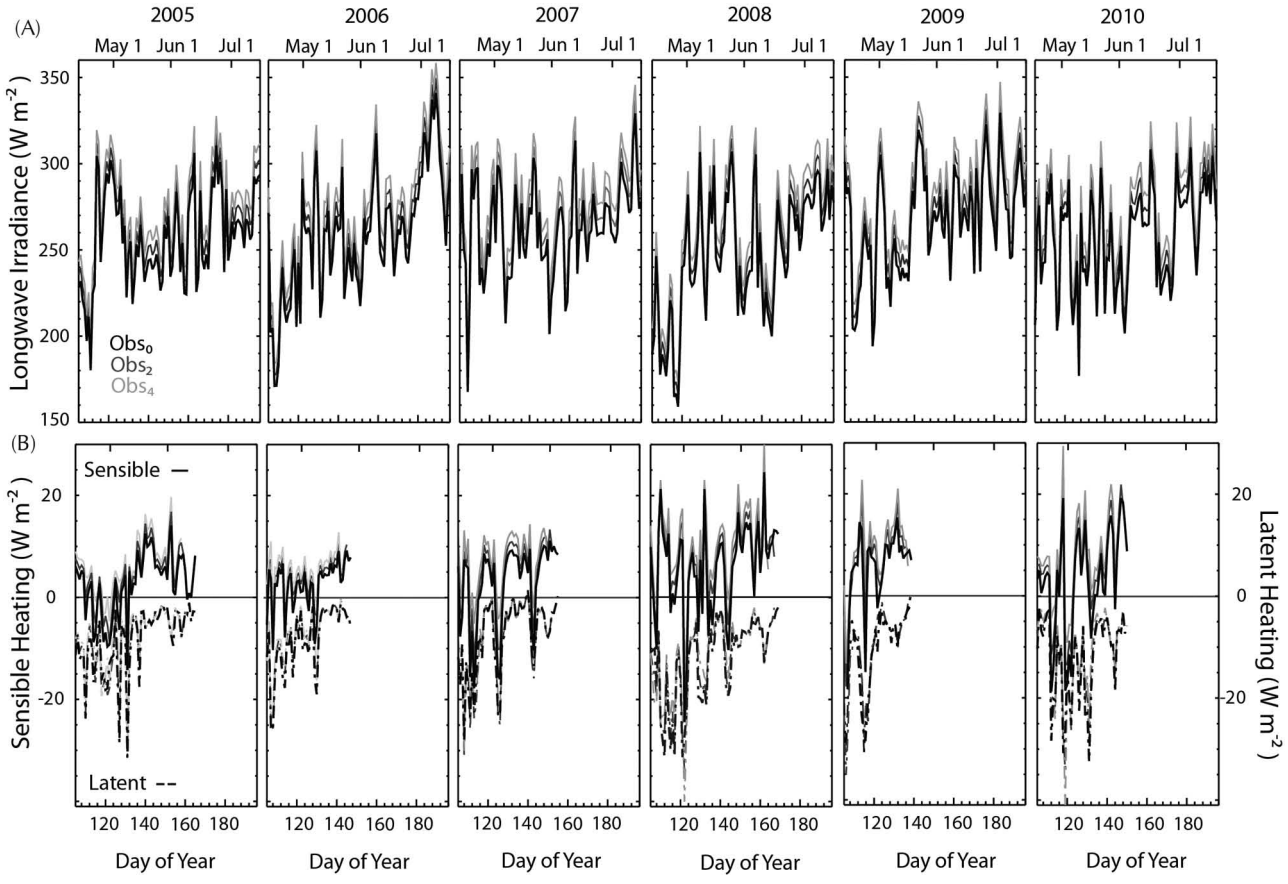

Figure 4. Time series of daily mean (a) longwave irradiance and (b) sensible heating and latent heating, for 2005 through 2010. Observed longwave irradiance is recorded at the subalpine tower; increases in downwelling longwave with temperature increases of 2°C and 4°C are shown by the lighter gray lines. Sensible and latent heating are simulated by SNOBAL. Lines end on modeled SAG date.

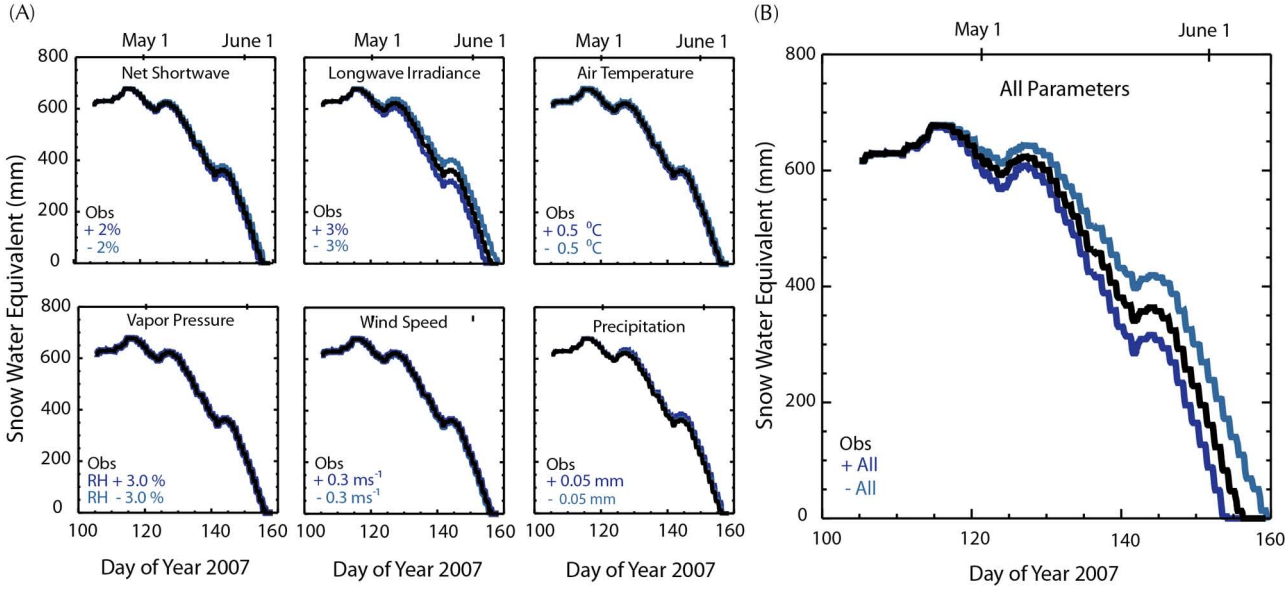

Figure 5. Modeled daily mean SWE evolution for ranges in (a) instrument accuracy and (b) maximum total uncertainty due to instrumentation measurement.

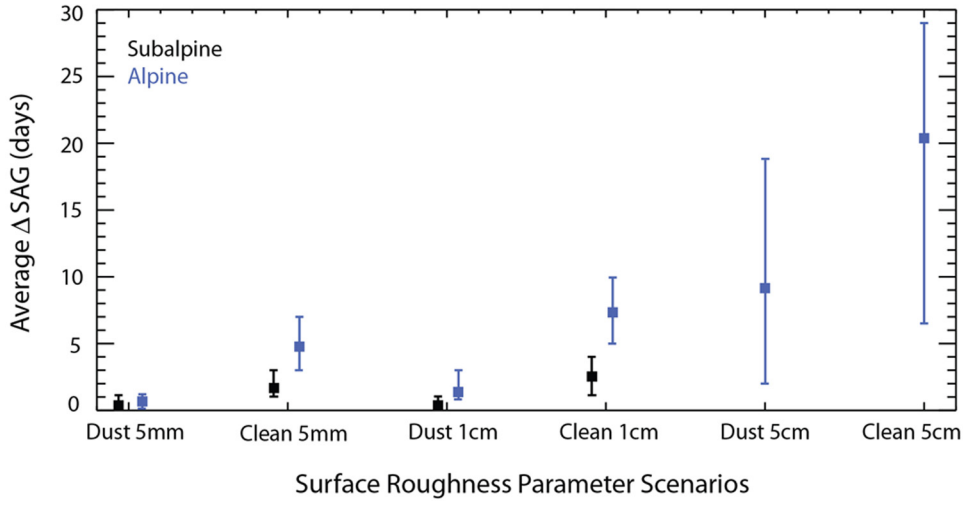

Figure 6. Average change in snow-all-gone date (ΔSAG) relative to the standard 1 mm roughness value for variations to the SNOBAL surface roughness parameter, error bars show maximum and minimum number of advanced days melt.

clean case at both sites, for a modeled clean snowpack increases in surface roughness can enhance melt by 3 to 7 days at the alpine site and 1 to 4 days at the subalpine site. The cumulative impacts from increased turbulent transfer at the surface in the presence of dust are reduced due to shorter snow duration.

[26] At the alpine site a marked increase in ΔSAG occurs between 1 and 5 cm increased surface roughness where large difference in melt-out date occurs. The larger ΔSAG for 1 and 5 cm roughness occur for both the dust and clean cases, driven by greater wind speeds in the alpine. The use of 1 mm constant surface roughness in the model is reasonable as these results indicate the model is not highly sensitive to changes in surface roughness until roughness values increase beyond those commonly observed for alpine snow cover in general, and for observed surface roughness at both of our study sites.

3.5. Snow Cover Duration

[27] We present the time series of snow water equivalent during the ablation seasons of 2005 through 2010 for the subalpine and alpine site (Figure 7). The ablation season is defined here as that between 15 April (near average peak SWE for the region) and date of SAG.

[28] The clean snowpack is modeled by removing the minimum and maximum RF due to dust, then averaging the daily values of these two scenarios to represent a conservatively clean snowpack (C_0); without direct observation of zero-dust conditions, this is our best understanding of the evolution of the snowpack in the absence of dust. The difference between when the D_0 and C_0 time series arrive at SAG ($\Delta SAG_{D_0,C_0}$) indicates the number of days that dust RF advances complete melt under observed meteorological conditions.

[29] The greatest $\Delta SAG_{D_0,C_0}$ of 51 days (subalpine) and 44 days (alpine) occurred in 2009 when the end of year dust concentration was 5–20× greater than concentrations in 2005 through 2008. The next largest divergence of 48 days (subalpine) and 37 days (alpine) occurred in 2010, the next largest dust concentration year. The years with lower dust concentrations; 2005, 2007, and 2008 still show $\Delta SAG_{D_0,C_0}$ of 28–34 days (subalpine) and 23–27 days (alpine).

[30] Dust radiative forcing exerts its strongest impact on ΔSAG in years with greater SWE accumulation, as dust-driven divergence in melt rates has more mass over which to influence duration of snow cover [*Painter et al.*, 2007]. This is illustrated by a comparison of 2005 (a high SWE, low dust year) and 2006 (low SWE, high dust). In 2005, $\Delta SAG_{D_0,C_0}$ was 28 days (subalpine) and 23 days (alpine), whereas for 2006 the $\Delta SAG_{D_0,C_0}$ was 31 days (subalpine) and 21 days (alpine). At the alpine site this was the smallest difference between the D_0 and C_0 cases, even though 2006 had a higher end-of-year dust concentration than did 2005. The higher peak SWE in 2005 relative to 2006 resulted in the small difference in $\Delta SAG_{D_0,C_0}$ between the two years despite the increase in dust concentration and radiative forcing in 2006. A larger $\Delta SAG_{D_0,C_0}$ would have been possible in 2006 with greater SWE accumulation.

[31] While there is interannual variability in the influence of dust RF on SAG, over the 6-year record, $\Delta SAG_{D_0,C_0}$ can appear to increase linearly with the end-of-year dust concentration for each site (Figure 8; R^2 values of 0.94 and 0.95 at the subalpine and alpine site, respectively). However, given the nonlinear response of reduction of albedo to increases in dust concentration, we would expect that the relationship between $\Delta SAG_{D_0,C_0}$ and dust concentration would likewise be nonlinear. Indeed, with the subalpine and alpine data taken together, the plot of $\Delta SAG_{D_0,C_0}$ to dust concentration suggests a logarithmic form, which is more consistent with our understanding of optical responses. Future data from the SBBSA will allow us to more robustly populate this plot.

3.6. Influence of Temperature Increases

[32] The differences of C_2, and C_4 SAG from C_0 SAG (Figure 7) indicate the number of days that the temperature increases would advance loss of snow cover in the absence of dust ($\Delta SAG_{C_2,C_0}$ and $\Delta SAG_{C_4,C_0}$, respectively). The

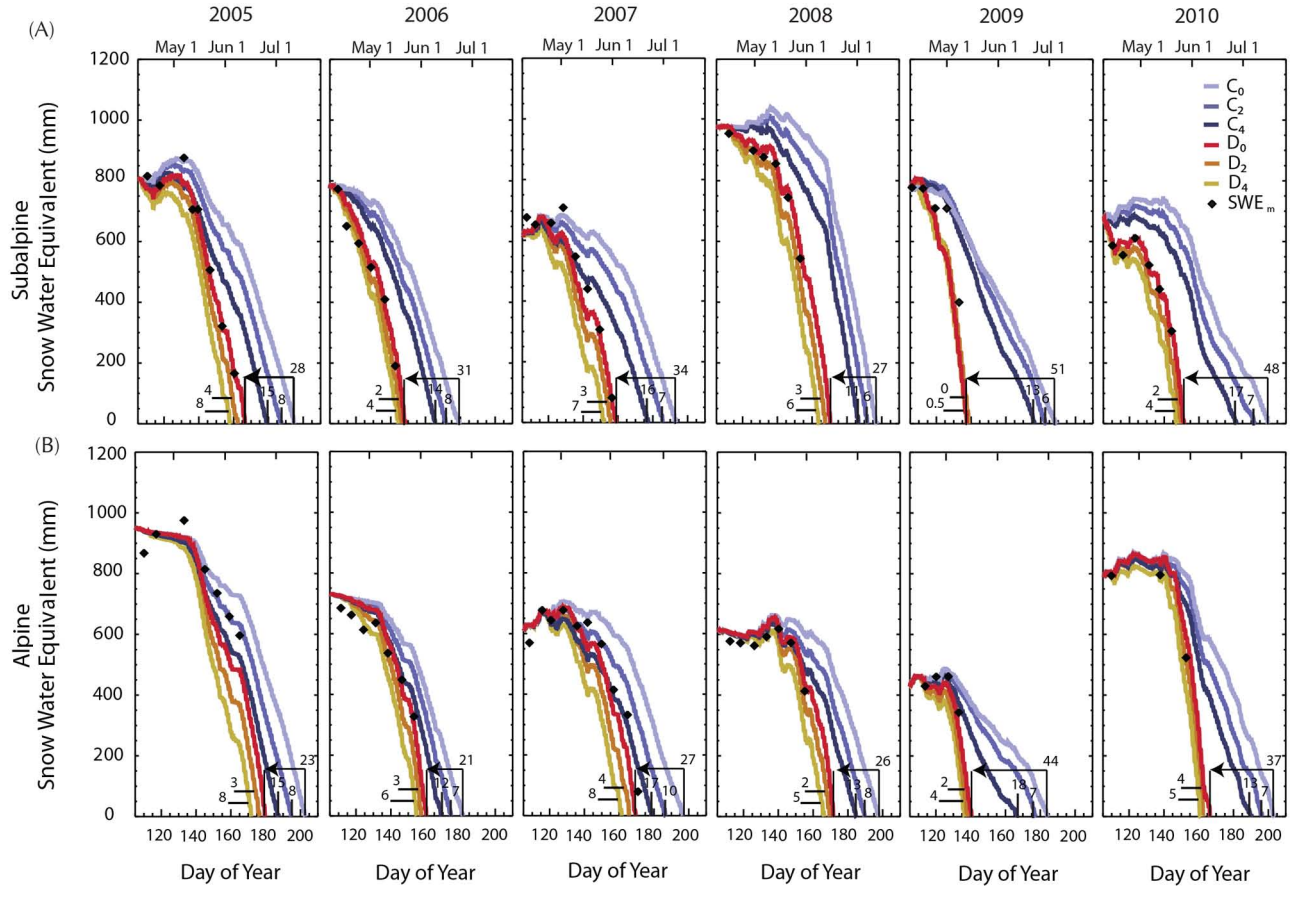

Figure 7. Daily mean SWE during the ablation season at the (a) subalpine and (b) alpine for all scenarios. Numbers by the C_2, C_4, and D_0 indicate number of days advanced melt from the C_0 case. Numbers by the D_2 and D_4 curves represent advanced melt from the D_0 case. Modeled SWE for D_0 closely matches point measurements of SWE (black triangles) for observed conditions (red curve) in almost all cases.

differences of D_2 and D_4 SAG from D_0 SAG represent the number of days temperature increases would further shorten snow cover in the presence of dust ($\Delta SAG_{D_2,D_0}$ and $\Delta SAG_{D_4,D_0}$, respectively).

[33] Temperature increases of 2°C and 4°C under dust-free scenarios induce $\Delta SAG_{C_2,C_0}$ and $\Delta SAG_{C_4,C_0}$ of 6 to 18 days—a lesser melt forcing than the observed dust radiative forcing in this region (21 to 51 days). Combined with

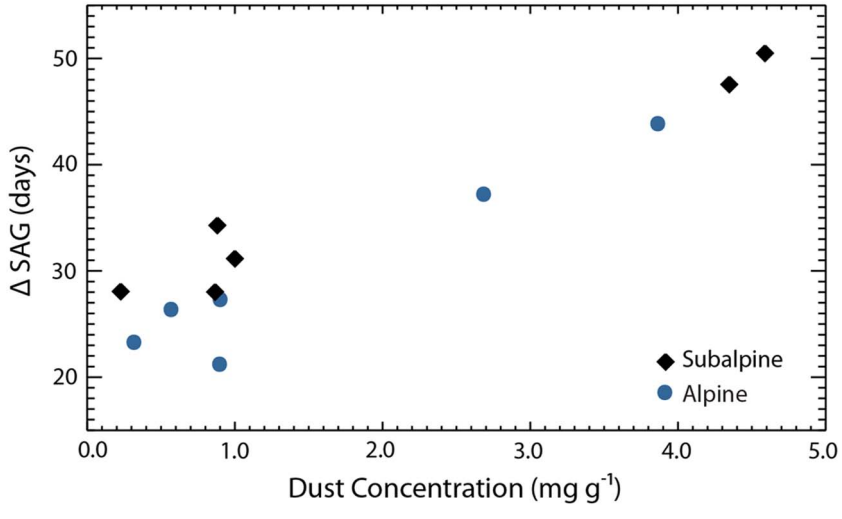

Figure 8. Change in snow-all-gone date (ΔSAG) with end of year dust concentrations. R^2 values are 0.94 and 0.92 at the subalpine and alpine site, respectively.

observed dust conditions, the increases in temperature shortened snowcover duration by 0 to 8 additional days ($\Delta SAG_{D_2,D_0}$, $\Delta SAG_{D_4,D_0}$). The reduced impact of increased temperature under dusty conditions is due to the reduced snow cover duration over which the increased sensible heating and longwave irradiance can affect a difference in SAG. The lowest melt forcing by increased temperature in the dusty case occurred in 2009 at the subalpine site, corresponding to the greatest mean dust radiative forcing. In these scenarios, $\Delta SAG_{D_2,D_0}$, $\Delta SAG_{D_4,D_0}$ were <1 day.

3.7. Snowpack Outflow

[34] In addition to SWE, daily mean "snowpack outflows" were also modeled (Figure 9). Because SNOBAL simulates only melt and sublimation at a point and does not account for infiltration into the soil column, transpiration by vegetation in or near the snow column, etc., we refer to the water leaving the bottom of the snowpack as outflow.

[35] Generally, the dust-driven outflows have a quasi-monotonic increase to a higher peak at the end of snow cover, and then melt-out occurs within days—on average 2.5 (subalpine) to 3.5 days (alpine) after peak outflow. The clean snow cases reach a lower peak 1 to 2 weeks after the dust cases with a less rapid decrease to melt-out, on average 19 (subalpine) to 13 days (alpine) after peak outflow occurs, as energy fluxes to the surface decrease. In 2006, a rain-on-snow event was predicted for the C_4 scenario at the subalpine site (after melt-out in the dust cases). This was modeled as snow for other scenarios and produced a peak outflow higher than any of the dust peaks. Similar late season rain-on-snow events with smaller magnitude also occur in 2009 at the subalpine site and 2010 at both sites. These are functions of air temperature and precipitation phase change prediction by the model, which utilizes temperature during precipitation events to determine precipitation type.

[36] In all years at both sites, annual outflow flux in the dust cases exceeds that of the clean cases (Figure 10). In the heaviest dust concentration year (2009), the D_0 outflow (0.97 kg m^{-2}) was more than double the C_n outflow (0.44 kg m^{-2}) at the subalpine site. On average, D_0 outflow over all years is 0.71 and 0.49 kg m^{-2} (subalpine, alpine), whereas average C_n outflow is 0.39 and 0.27 kg m^{-2} (subalpine, alpine).

[37] The variation in timing of peak outflow between dust and clean scenarios has implications for water resources and water resource management. In addition to danger from flooding, higher melt rates and increases in the magnitude of peak runoff can impact soil moisture storage and reduce the time period over which critical water management decisions are made. A longer snow-free season likely increases the amount of water lost to evapotranspiration and reduces available water supply [*Painter et al.*, 2010]. This is especially pertinent in this region as the majority of flow in the Colorado River comes from the melting of high

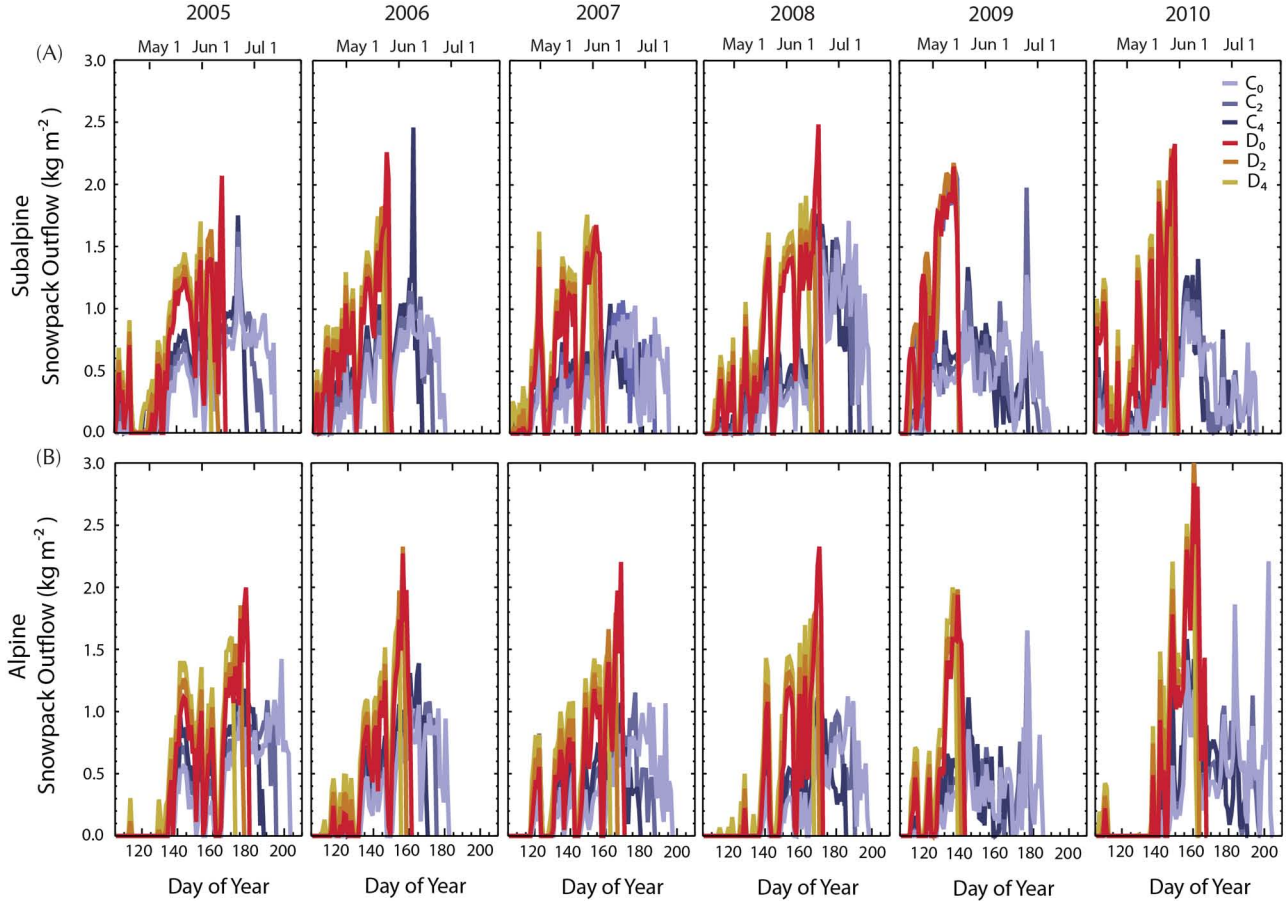

Figure 9. Time series of daily mean snowpack outflow over the ablation season at (a) subalpine and (b) alpine sites for all scenarios.

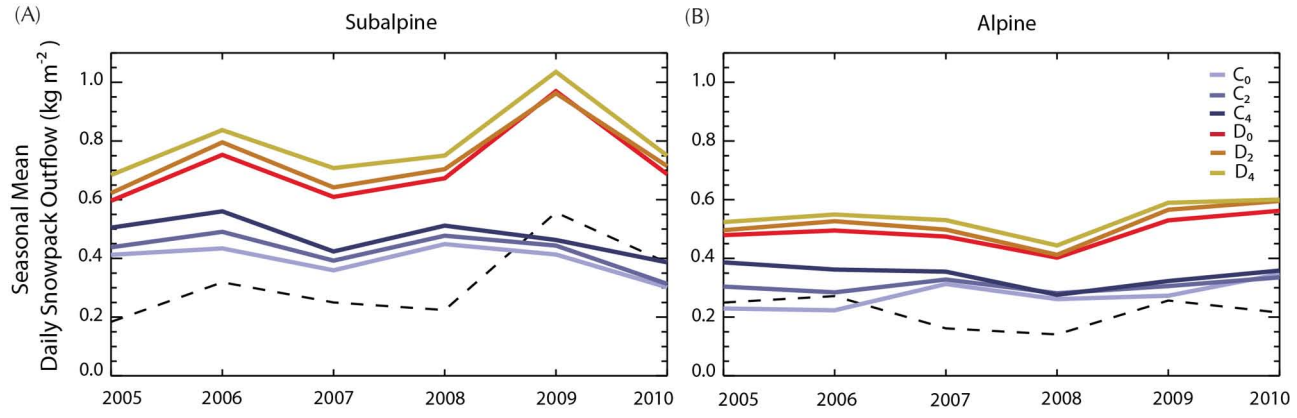

Figure 10. Mean daily snowpack outflow for all scenarios at the (a) subalpine and (b) alpine, with the difference between the D_0 and C_0 snowpack outflows represented by the dashed line.

elevation snow cover [*Christensen et al.*, 2004]. Water availability may also be impacted if the majority of the water melts over a shorter period of time and there is insufficient reservoir storage to hold the accelerated flow and reservoir spillage is unavoidable. Additionally, earlier removal of snow cover coupled with increasing temperature has the potential to impact alpine vegetation patterns, with a shift toward earlier, more spatially coincident greening and flowering [*Steltzer et al.*, 2009].

4. Concluding Remarks

[38] Modern levels of dust deposition on the mountain snowpack are a relatively new phenomenon in this region over the last 150 years [*Neff et al.*, 2008; *Painter et al.*, 2010]. Over the 6-year record at our study area we have observed an increase in the number of dust events with substantial interannual variability in dust loading. *Painter et al.* [2007] found that dust in snow advanced melt-out date by up to 35 days in the springs of 2005 and 2006. We find that in high dust concentration years melt-out date can be advanced by up to 51 days.

[39] Enhanced snowmelt rates increase the rate of snowpack outflow, which can impact water supply operations. Faster melt also lengthens the snow-free season, when evapotranspiration rates are highest. *Painter et al.* [2010] found that dust RF impacts annual runoff volume of the Colorado River at Lee's Ferry, AZ, by 5% (~1.0 billion m^3) on average. Their study was conducted using a snow albedo parameterization that comes from 2005–2008, and does not include the exceptionally low albedos observed in 2009 and 2010—thus the runoff impacts of dust deposition may be even greater than estimated.

[40] While our results indicate that temperature does not have as large an impact on melt in the presence of dust we recognize that this is a relatively simple treatment of temperature increase and emphasize that this study investigates the relative forcings of snowmelt by dust radiative forcing and temperature increases for the same snowpack and only in the snowmelt season. These results do not address how climate change may impact alpine snow cover in other areas that do not experience as high of dust concentrations, neither does it address other impacts such as changing precipitation patterns and more precipitation falling as rain rather than snow that would result from a warming climate.

[41] Over our relatively short record we have observed that dust deposition can be highly variable; as discussed above, at our sites the number of dust deposition events increased during the period 2005 through 2010, yet dust concentrations have varied by more than an order of magnitude during those years but not in concert with the steady increase in number of events. This is due in part because climate, land cover, and atmospheric circulation, which vary at multiple spatial and temporal scales, impact dust emission and loading. In addition to natural variability, human impacts such as changes in land use are contributing to changes in dust emission. This variability may increase with ongoing regional warming. Warming in the southwestern US is likely to increase dust emission and loading to the mountains of the CRB through drought, disturbance, and desertification [*Munson et al.*, 2011]. It is important to understand the interannual variability of dust deposition to the mountain snow cover to better understand the potential long-term impacts. The results presented here have important implications not just for runoff timing and magnitude and water supply management, but also for power generation, alpine phenology, forest fire regimes, and recreation interests.

[42] **Acknowledgments.** This work was funded by the National Science Foundation grants ATM04323237 and ATM0431955, and NASA project NNX10AO97G. We acknowledge the assistance of Andrew Barrett in data processing. Part of this work was performed at the Jet Propulsion Laboratory, California Institute of Technology under a contract with NASA. We thank Jeff Dozier, Steve Warren, and an anonymous reviewer for their suggestions that improved this manuscript.

References

Ball, F. K. (1954), Dirt polygons on snow, *Weather*, *9*, 322–323.

Barnett, T. P., and D. W. Pierce (2009), Sustainable water deliveries from the Colorado River in a changing climate, *Proc. Natl. Acad. Sci. U.S.A.*, *106*, 7334–7338, doi:10.1073/pnas.0812762106.

Brock, B. W., I. C. WIllis, and M. J. Sharp (2006), Measurement and parameterization of aerodynamic roughness length variations at Haut Glacier d'Arolla, Switzerland, *J. Glaciol.*, *52*, 675–688, doi:10.3189/172756500781832675.

Christensen, N. S., A. W. Wood, D. P. Lettenmaier, and R. N. Palmer (2004), Effects of climate change on the hydrology and water resources of the Colorado River Basin, *J. Hydroclimatol.*, *62*, 337–363.

Fassnacht, S. R., M. W. Williams, and M. V. Carrao (2009), Changes in the surface roughness of snow from millimetre to metre scales, *Eco. Complex.*, *6*, 221–229, doi:10.1016/j.ecocom.2009.05.003.

Hansen, J., and L. Nazarenko (2004), Soot climate forcing via snow and ice albedos, *Proc. Natl. Academy Sci. U.S.A.*, *101*, 423–428.

Jackson, B. S., and J. J. Carroll (1978), Aerodynamic roughness as a function of wind direction over asymmetric surface elements, *Bound.-Layer Meteorol.*, *14*, 323–330, doi:10.1007/BF00121042.

Konzelmann, T., R. S. W. van de Wal, W. Greuell, R. Bintanja, E. A. C. Henneken, and A. Abe-Ouchi (1994), Parameterization of global and longwave incoming radiation for the Greenland Ice Sheet, *Global Planet Change*, *9*, 143–164, doi:10.1016/0921-8181(94)90013-2.

Marks, D., and J. Dozier (1992), Climate and energy exchange at the snow surface in the alpine region of the Sierra Nevada 2. Snow cover energy balance, *Water Resour. Res.*, *28*, 3043–3054.

Marks, D., J. Dozier, and R. E. Davis (1992), Climate and energy exchange at the snow surface in the alpine region of the Sierra Nevada 1. Meteorological measurements and monitoring, *Water Resour. Res.*, *28*, 3029–3042.

Marks, D., J. Kimball, D. Tingey, and T. Link (1998), The sensitivity of snowmelt processes to climate conditions and forest cover during rain-on-snow: A case study of the 1996 Pacific Northwest flood, *Hydrol. Processes*, *12*, 24.

Munson, S. M., J. Belnap, and G. S. Okin (2011), Responses of wind erosion to climate-induced vegetation changes on the Colorado Plateau, *Proc. Natl. Acad. Sci. U.S.A.*, *108*, 3854–3859, doi:10.1073/pnas.1014947108.

Neff, J. C., A. P. Ballantyne, G. L. Farmer, N. M. Mahowald, J. L. Conroy, C. C. Landry, J. T. Overpeck, T. H. Painter, C. R. Lawrence, and R. L. Reynolds (2008), Increasing eolian dust deposition in the western United States linked to human activity, *Nat. Geosci.*, *1*, 189–195, doi:10.1038/ngeo133.

Painter, T. H. (2011), Comment on: S. K. Singh, Anil V. Kulkarni, and Bajrang S. Chaudhary, Hyperspectral analysis of snow reflectance to understand the effects of contamination and grain size, Annals of Glaciology 51(54) 2010, *J. Glaciol.*, *57*, 183–185, doi:10.3189/002214311795306646.

Painter, T. H., A. P. Barrett, C. C. Landry, J. C. Neff, M. P. Cassidy, C. R. Lawrence, K. E. McBride, and G. L. Farmer (2007), Impact of disturbed desert soils on duration of mountain snow cover, *Geophys. Res. Lett.*, *34*, L12502, doi:10.1029/2007GL030284.

Painter, T. H., J. S. Deems, J. Belnap, A. F. Hamlet, C. C. Landry, and B. Udall (2010), Response of Colorado River runoff to dust radiative forcing in snow, *Proc. Natl. Acad. Sci. U.S.A.*, *107*, 17125–17130, doi:10.1073/pnas.0913139107.

Painter, T. H., S. M. Skiles, J. S. Deems, A. C. Bryant, and C. C. Landry (2012), Dust radiative forcing in snow of the Upper Colorado River Basin: 1. A 6 year record of energy balance, radiation, and dust concentrations, *Water Resour. Res.*, *48*, W07521, doi:10.1029/2012WR011985.

Pluss, C., and R. Mazzoni (1994), The role of turbulent heat fluxes in the energy balance of high Alpine snow cover, *Nord. Hydrol.*, *25*, 25–38, doi:10.2166/nh.1994.002.

Poggi, A. (1976), Heat balance in the ablation area of the Ampere Glacier (Kerguelen Islands), *J. Appl. Meteorol.*, *16*, 48–55, doi:10.1175/1520-0450.

Rhodes, J. J., R. L. Armstrong, and S. G. Warren (1987), Mode of formation of "ablation hollows" controlled by dirt content of snow, *J. Glaciol.*, *33*, 135–139.

Sedlar, J., and R. Hock (2009), Testing longwave radiation parameterizations under clear and overcast skies at Storglaciären, Sweden, *The Cryosphere*, *3*, 75–84, doi:10.5194/tc-3-75-2009.

Singh, S. K., A. V. Kulkarni, and B. S. Chaudhary (2010), Hyperspectral analysis of snow reflectance to understand the effects of contamination and grain size, *Ann. Glaciol.*, *51*, 83–88, doi:10.3189/172756410791386535.

Steltzer, H., C. C. Landry, T. H. Painter, J. Anderson, and E. Ayres (2009), Dust-induced early snowmelt synchronizes phenology across an alpine landscape, *Proc. Natl. Acad. Sci. U.S.A.*, *106*, 11629–11634, doi:10.1073/pnas.0900758106.